ADVANCED MATERIALS

DOI: 10.1002/adma.200800214

High Tensile Ductility and Strength in Bulk Nanostructured Nickel**

By *Yonghao Zhao, Troy Topping, John F. Bingert, Jeremy J. Thornton, Andrea M. Dangelewicz, Ying Li, Wei Liu, Yuntian Zhu, Yizhang Zhou,* and *Enrique J. Lavernia**

Bulk nanostructured (NS) materials have relatively high strength but disappointingly low tensile ductility (elongation to failure) at ambient temperatures.[1–4] The limited ductility of NS materials has emerged as a particularly challenging issue in the study and application of this novel class of materials. Recently, a variety of strategies aimed at improving the poor ductility of NS materials have been reported; the results reveal varying degrees of success.[5,6] Despite some encouraging reports, the improvements in ductility remain quite limited, usually below 15% for most of the strategies, except possibly for bi-modal Cu (with a ductility of 65%) and ultrafine grained (UFG) Fe-Cr-Ni-Mn steel (ca. 30%).[7,8] In this Communication, we use cryomilling and subsequently quasi-isostatic (QI) forging processes (formerly known as Ceracon forging), to prepare bulk dense multimodal and bimodal NS Ni with tensile ductility of 42% and 49%, and yield strengths of 457 and 312 MPa, respectively. This combination of strength and ductility is much superior to those of the NS Ni prepared by electro-deposition (ED),[9–16] cryorolling,[17] equal-channel angular pressing (ECAP) and high pressure torsion (HPT) methods,[18] and cold drawing.[19] Microstructural analyses suggest that significantly reduced extrinsic processing artifacts, the presence of equilibrium high-angle grain boundaries (including twin boundaries), and multi-/bimodal grain size distributions are responsible for the measured high ductility. The high strength is argued to originate from several sources, including a high density of dislocations, UFGs, and from solid solution strengthening. Compared with other synthesis methods, the synthesis methodology described in the present work has no scale or material limitations, and therefore has important implications in terms of its potential for the large-scale fabrication of bulk NS metals, alloys, and composites that can be used in applications requiring both high ductility and strength.

Bulk NS materials are usually synthesized by either a two-step approach involving the synthesis and consolidation of nanoparticles (e.g., via inert-gas condensation)[2,3] or nanocrystalline powders (e.g., via ball milling or cryomilling),[20] or a one-step approach such as severe plastic deformation (SPD).[21] In the case of NS materials prepared by the two-step approach, powder handling can yield extrinsic processing artifacts (such as porosity, incomplete bonding, impurities, and others). It is now well-established that these artifacts, when present, will cause premature failure under tensile stresses, sometimes even before the onset of yielding.[3] In a recent study, the material was consolidated in situ via an approach involving cryomilling followed by room-temperature milling.[22] In this case, the NS Cu prepared by this novel method was reported to have a uniform tensile elongation (strain before necking) of 14% and a high yield strength of 790 MPa. Despite these encouraging results, this approach has material and scale limitations: the NS spheres are limited to a size comparable to that of the milling media, and it is only applicable to metals with low melting points that can be welded into dense spheres at room temperature. Moreover, the structural features responsible for this excellent strength and ductility behavior are not fully understood, and this has hindered the search for procedures that may be used effectively to improve the ductility of NS materials.

The one-step SPD approaches can be used to synthesize flaw-free NS materials with higher ductility than those synthesized by the two-step approach. However, even these NS materials often exhibit a very low or near-zero uniform tensile elongation owing to their low strain hardening (dislocation storage capacity). Several different strategies have recently been developed to improve the poor ductility of NS materials; these include approaches such as the introduction of a bimodal grain size distribution,[7,20] or pre-existing nanoscale twins,[23,24] using dispersions of nanoparticles/-precipitates,[25,26] preparing a mixture of two or multiple phases,[27,28] transformation-/twinning-induced plasticity,[8,29] and changing the deformation conditions.[30,31] Despite varying degrees of success, most of the strategies have inherent processing and/or material limitations. The objective of the present study was two-fold: First, to explore a generic synthesis

[*] Prof. E. J. Lavernia, Dr. Y. H. Zhao, T. Topping, Dr. Y. Li, W. Liu, Dr. Y. Z. Zhou
Department of Chemical Engineering and Materials Science
University of California
Davis, CA 95616 (USA)
E-mail: lavernia@ucdavis.edu
Dr. J. F. Bingert, J. J. Thornton, A. M. Dangelewicz, Prof. Y. T. Zhu
Los Alamos National Laboratory
Los Alamos, NM 87545 (USA)
Prof. Y. T. Zhu
Department of Materials Science & Engineering
North Carolina State University
Raleigh, NC 27695-7919 (USA)

[**] This project is supported by the Office of Naval Research (Grant number N00014-04-1-0370) with Dr. Lawrence Kabacoff as program officer. Supporting Information is available online from Wiley InterScience or from the authors.

WILEY InterScience® DISCOVER SOMETHING GREAT

© 2008 WILEY-VCH Verlag GmbH & Co. KGaA, Weinheim

approach that can be used to prepare bulk NS materials with both high ductility and high strength. Second, to provide fundamental insight into the mechanisms that govern the high ductility in NS materials.

Two pure NS Ni samples with multi- and bimodal grain size distributions were prepared by cyomilling and subsequent QI forging processes, conducted at Advanced Materials and Processing Technologies, LLC (AM^2T) in Riverbank, CA (USA). The QI forging process is a hot consolidation technique that utilizes a granular pressure transmission medium (PTM) to distribute some of the compressive load to all sides of the part being consolidated. The PTM enables a great degree of freedom in the shapes to be processed and achieves full-density parts.[32] Nanocrystalline Ni powders with a grain size of approximately 10 nm were prepared by cryomilling commercially pure Ni powders (>99.7 wt %) in liquid nitrogen.[33] The cryomilled Ni powders were placed in stainless steel can and degassed, first at a temperature of 450 °C for 24 hours followed by a second degassing step at a temperature of 810 °C for 2.5 hours. The degassed cans were then QI forged at 800 °C to form bulk dense NS Ni with a purity of 99.3% (Supporting Information Tables 1 and 2), a density of 8.87 g cm^{-3} (99.6% of Ni's theoretical density), and a multimodal grain size distribution. The bulk bimodal NS Ni was prepared by degassing and QI forging a mixture of the cryomilled powders (50%) and as-received coarse-grained (CG, 50%) Ni powders under the same conditions. The purity and density of the bimodal NS Ni are 99.7% and 8.85 g cm^{-3}, respectively. For comparison purposes, a portion of the multimodal NS Ni was annealed at 1000 °C for 10 hours to form CG Ni reference with an average grain size of about 15 μm (Supporting Information Fig. S1).

The engineering tensile stress–strain curves of the multimodal (designated as multi-Ni) and bimodal NS Ni (bi-Ni), as well as the curve of the CG Ni reference material, are compared in Figure 1a. It is apparent that the multi-Ni shows a remarkable combination of ductility and strength, yielding at 457 MPa with 42% ductility at a tensile strain rate of $10^{-2}\,s^{-1}$. The bi-Ni shows lower strength and higher ductility, yielding at 312 MPa with 49% ductility. In contrast, the CG Ni exhibits a yield strength of 154 MPa and ductility of 48%. It is interesting that the bi-Ni sample has a high ductility comparable to the CG Ni. As listed in Table 1, the yield strength of the multi-Ni has no strain rate dependence over the range of $10^{-4}\,s^{-1}$ to $10^{-2}\,s^{-1}$. This trend can be further confirmed by compressive test results (Supporting Information Fig. S2). The uniform elongation ε_{ue} of the bi-Ni (28%) is larger than that of the multi-Ni (24%), smaller than that of the CG Ni (34%). This indicates that the high ductility of the bi-Ni originates from its larger post-necking elongation, suggesting greater rate sensitivity compared to CG Ni. The CG Ni sample has a higher normalized strain hardening rate Θ as compared to that of bi-Ni, which in turn has a higher Θ than that of the multi-Ni (Supporting Information Fig. S3). Both Θ and ε_{ue} have the same variation sequences.

The multi-Ni and bi-Ni samples, as well as the CG Ni fractured via ductile mechanisms, as verified by their large reductions of fracture areas A and the numerous dimples over the entire fracture surface (Supporting Information Figs. S4 and S5). As listed in Table 1, the variation sequence of A is the same as that of the ductility, that is, multi-Ni < CG Ni < bi-Ni. Both multi-Ni and bi-Ni samples shear fractured with a fracture angle θ of about 50 °, while the CG Ni failed in a normal tensile fracture mode ($\theta = 90$ °, Supporting Information Fig. S4). The shear fracture is attributable to the nanostructures which resulted in a decreased ratio of the average critical normal fracture stress to shear fracture stress.[34] The dimples in the multi-Ni and bi-Ni are smaller than those in CG Ni owing to their smaller grains, and elongated owing to void nucleation and subsequent coalescence via shear fracture (Supporting Information Fig. S5).

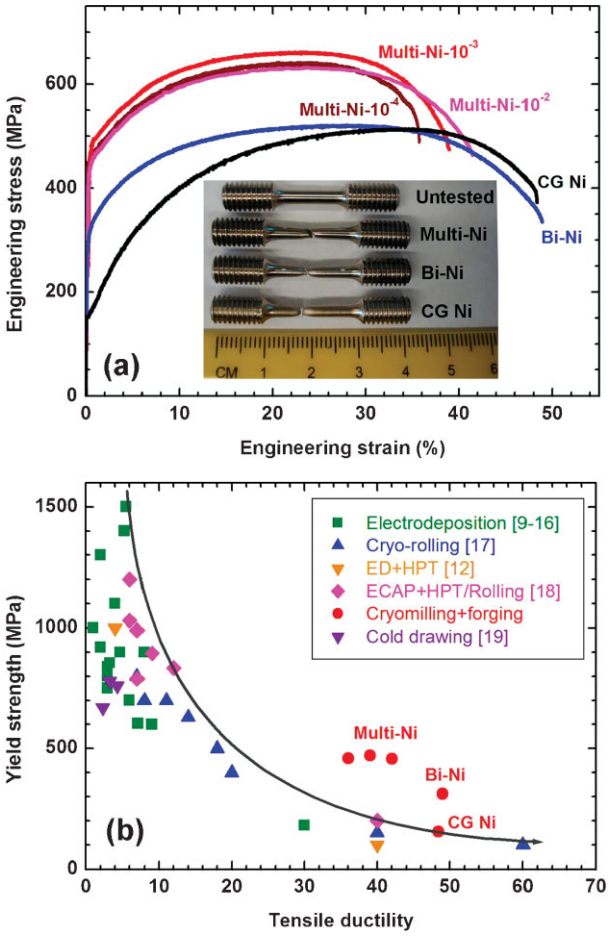

Figure 1. a) Tensile engineering stress–strain curves of the multimodal (Multi-Ni), bimodal NS Ni (Bi-Ni), and CG Ni samples. The multi-Ni was tested at three different strain rates: 10^{-2}, 10^{-3}, and $10^{-4}\,s^{-1}$, as indicated in the figure. The bi-Ni and CG Ni were tested at a strain rate of $10^{-3}\,s^{-1}$. The inset shows the picture of the fractured tensile specimens. b) Yield strength versus tensile ductility of NS Ni samples prepared by electrodeposition (ED) [9–16], cryo-rolling [17], equal-channel-angular (ECAP) and high pressure torsion (HPT) [18], cold drawing [19], as well as cryomilling and QI forging processes.

Figure 1b summarizes the yield strength versus tensile ductility, available from the literature, for NS Ni prepared by ED,[9–16] cryo-rolling,[17] ECAP and HPT,[18] cold drawing[19] as well as the present tensile results. It is apparent that all the

 © 2008 WILEY-VCH Verlag GmbH & Co. KGaA, Weinheim

ADVANCED MATERIALS

Table 1. Lists of tensile and compressive yield strengths $\sigma_{0.2}$, elongations to failure ε_{ef}, uniform elongations ε_{ue}, reductions of fracture areas A, and shear fracture angle θ of the multimodal (multi-Ni), bimodal NS Ni (bi-Ni), and the CG Ni samples with different strain rates.

Sample	Strain rates [s^{-1}]	$\sigma_{0.2}$ tensile [MPa]	$\sigma_{0.2}$ compressive [MPa]	ε_{ef}	ε_{ue}	A	θ
Multi-Ni	10^{-2}	457	458	42%	24%	55%	49°
	10^{-3}	471	–	39%	23%	50%	50°
	10^{-4}	459	463	36%	23%	49%	42°
Bi-Ni	10^{-3}	312	–	49%	28%	69%	52°
CG Ni	10^{-3}	154	–	48%	34%	67%	90°

literature data are located at the right-bottom corner, and approximately show an inverse relationship between the strength and ductility. However, the current results from the multi-Ni and bi-Ni stand out from the trend, suggesting a superior combination of mechanical properties with enhanced toughness.

The mechanical properties of bulk solids are controlled by their microstructures. Quantitative electron backscatter diffraction (EBSD) results are shown in Figure 2 for representative regions from the multi- and bi-Ni samples from top-view (perpendicular to the forging direction). The multi-Ni is composed of equiaxed grains with a size range from about 100 nm to 8 μm (Fig. 2a and c). The wide grain size distribution in multi-Ni is thought to originate mainly from the non-uniformities in microstructures and compositions of the cryomilled powders, which yielded a non-uniform grain growth during subsequent degassing process. The bi-Ni mainly contains grains with a wide size range from approximately 200 nm to 30 μm (Fig. 2b and c). Considering that the grain size that developed during grain growth remains below 8 μm (as seen for

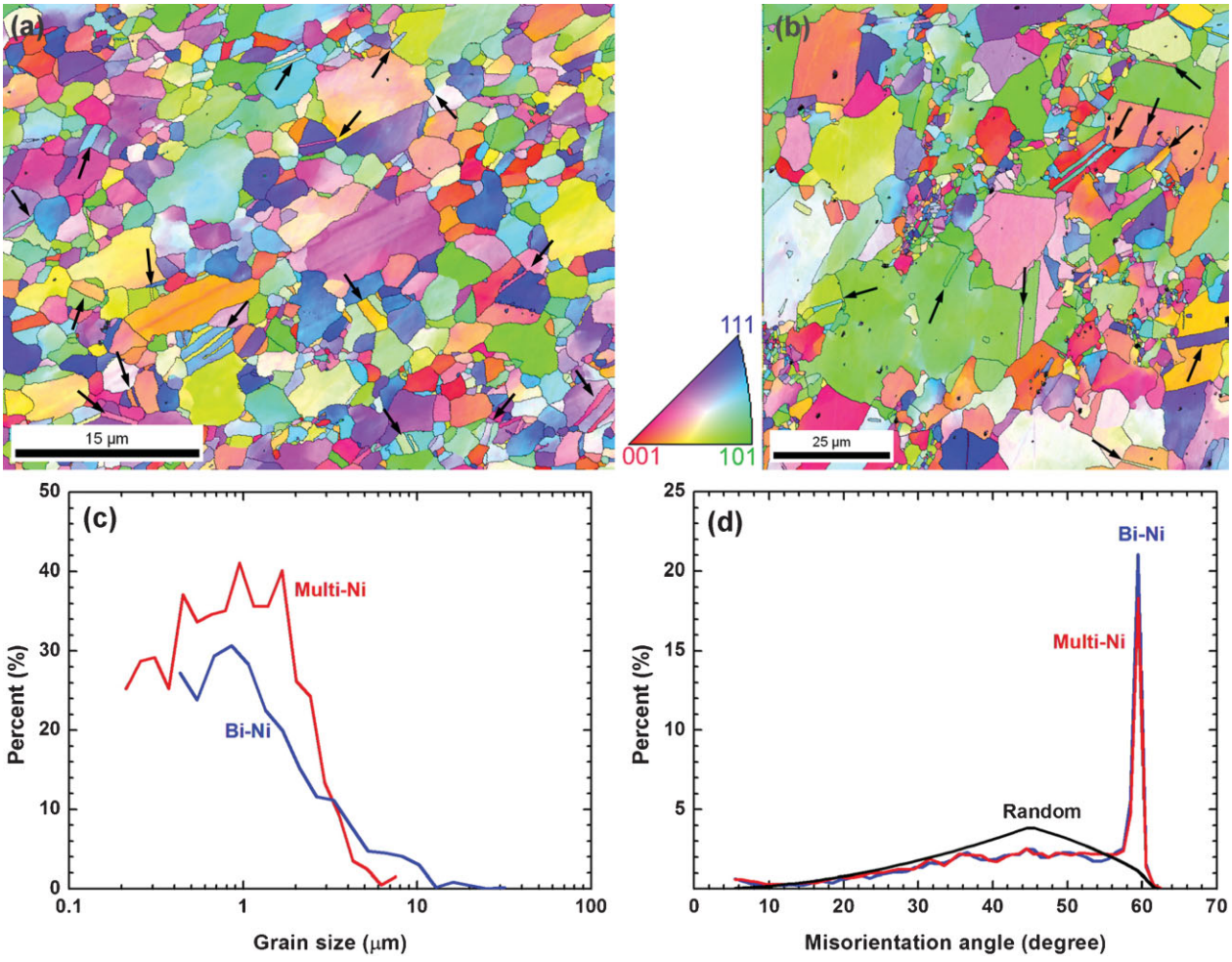

Figure 2. a,b) Representative EBSD images, c) grain size distribution, d) distribution of grain boundary misorientation angle for the multimodal (a) and bimodal NS Ni (b) samples from the top-view (perpendicular to the forging direction). The peak at about 60° is due to $\sum$3 coincident-site lattice twin boundaries. The twins in (a) and (b) are indicated by black arrows. The black dots in (a) and (b) are probably porosities. The black line in (d) represents a random misorientation distribution for a cubic polycrystal.

© 2008 WILEY-VCH Verlag GmbH & Co. KGaA, Weinheim

the multi-Ni), the grains larger than 8 μm in the bi-Ni are likely to originate from the as-received CG powders. The grains in both multi- and bi-Ni display an ill-defined texture suggestive of a small sampling from a random distribution (Supporting Information Fig. S6). Random textures would be expected from the nearly isostatic powder metallurgical processing. Grain sizes were determined using a 15° minimum misorientation boundary criterion, and included twins as grain boundaries (GBs). The average grain size, calculated as an equivalent diameter derived from areal orientation measurements, is 1.1 μm for the multi-Ni and 2.1 μm for the bi-NS Ni. However, the discrete step size used for EBSD mapping ranged from 75 nm to 130 nm, and therefore biased the statistics against any remnant grains of that dimension and smaller.

As illustrated in Figure 2a and b, twins are frequently observed in the microstructures of both samples. Twins usually terminate at the interior part of the coarse grains, and completely traverse the UFGs. In the case of the coarse grains, the twins probably formed during the QI forging process, whereas the twins in the UFGs may be both deformation twins and annealing growth twins formed during high-temperature degassing. The distributions of GB misorientation angles of the multi-Ni and bi-Ni are shown in Figure 2d. Considering all boundaries >5°, the high-angle grain boundaries (HAGBs, with misorientation angle >15°) in the multi-Ni sample comprise 96% of the total GB length, and the HAGB fraction in the bi-Ni is 95%. The large peak that appears at approximately 60° results from $\sum 3$ coincident-site lattice (CSL) twin boundaries, which include 22 and 26% for the multi-Ni and bi-Ni samples, respectively.

The above microstructural characteristics were further confirmed by transmission electron microscopy (TEM) studies. TEM observation shows that the majority of the GBs in these samples are straight, sharp, and clear, indicating that they are equilibrium GBs (Supporting Information Fig. S7). These equilibrium GBs are different from the wavy, diffuse, and ill-defined non-equilibrium GBs, which are the characteristic of the UFG materials processed via SPD method.[35,36] Twins were also frequently observed in both samples by TEM (Supporting Information Fig. S8).

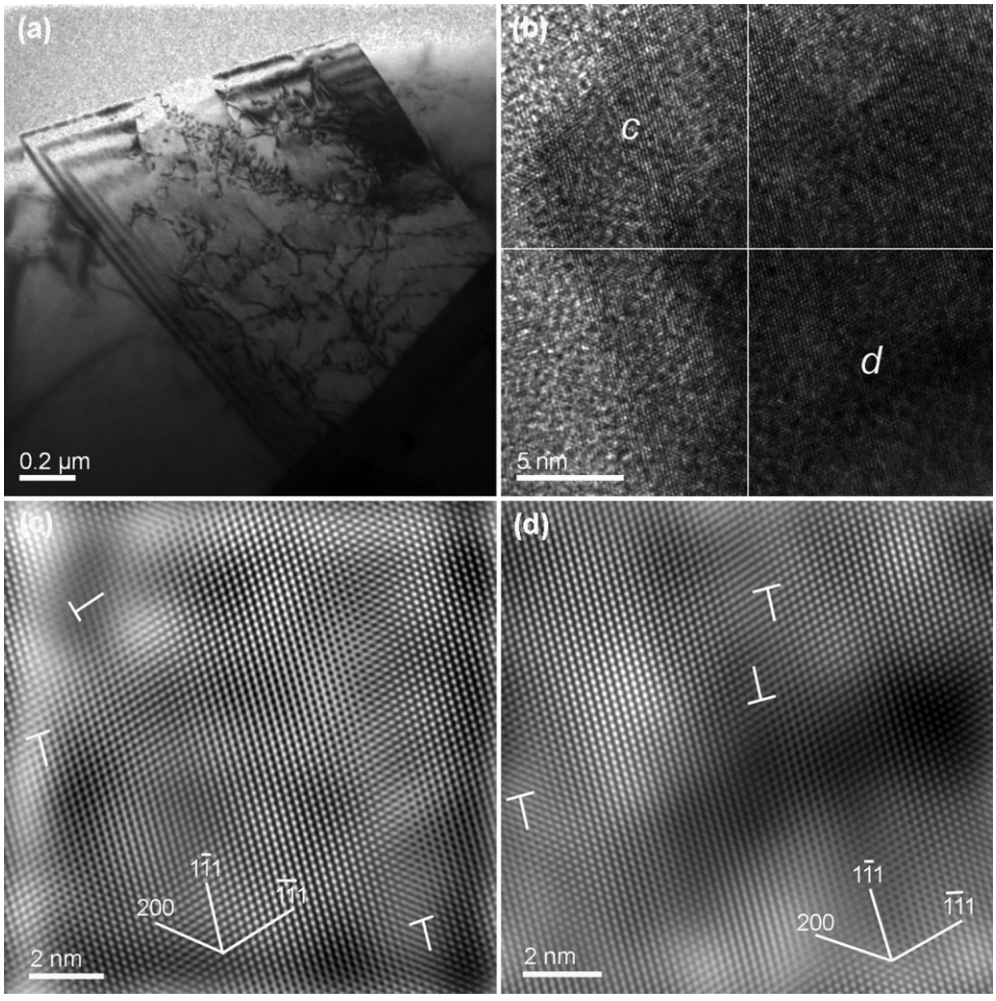

Figure 3. a) Typical bright-field TEM image of the multi-modal NS Ni sample showing dislocations within a grain. b) High-resolution TEM image from ⟨011⟩ zone axis. c,d) Inverse Fourier transforms of the areas marked *c* and *d* in (b) for the multi-modal NS Ni sample. Dislocation cores are marked by "T".

 © 2008 WILEY-VCH Verlag GmbH & Co. KGaA, Weinheim

ADVANCED MATERIALS

In addition to the microstructural characteristics previously described, TEM revealed a high density of dislocations in both multi-Ni and bi-Ni samples, as shown in Figure 3 and Supporting Information Figures S9 and S10. Different dislocation morphologies were observed, including dislocation tangling (Figs. 3a, S9a and b), cell structures (Figs S9a and b), dislocation networks (Fig. S9c and d) and low-angle GBs formed by dislocations (Fig. S10). The high density of dislocations was introduced during QI forge and therefore it exists within both large and small grains. Some of them dynamically recovered to form dislocation cells and small-angle GBs. The dislocation density estimated from the high-resolution TEM images (Fig. 3c and d) is about $1 \times 10^{16}\,m^{-2}$. Despite this high value, there is still space for multi- and bi-Ni to further accumulate dislocations as verified by their large strain hardening regions in the tensile stress–strain curves (Fig. 1a).

The high yield strength of the multi-Ni may be attributed to three factors: the UFGs, a high density of dislocations and Fe solid solution (0.44 wt %) strengthening. Moreover, the lower yield strength of the bi-Ni may be rationalized on the basis of its larger grain size and lower Fe concentration (0.19 wt %). High-temperature annealing significantly reduced the dislocation density and increased the grain size to about 15 μm, resulting in the observed much lower yield strength (154 MPa) in the CG Ni.

The measured high ductility may be attributed to the significantly reduced processing artifacts and the presence of a large fraction of HAGBs (including twin boundaries) as well as the multi-/bimodal grain size distributions. The QI forging process at high temperature significantly reduced the artifacts by providing large deformation space for the powder rearrangement. Earlier reports demonstrated that pre-existing twins and the large grains in bimodal grains are effective in blocking and storing dislocations, thereby yielding an improvement in the strain hardening rate.[7,20,23,24] The mechanisms responsible for increasing strain hardening owing to the presence of general HAGBs were discussed in Ref. [37] as (i) the HAGBs are more effective in blocking slipping dislocations, thereby forcing the dislocations to tangle and accumulate near the boundaries; and (ii) HAGBs sliding leads to dislocation emissions at triple junctions owing to the presence of high stress concentrations and these dislocations may act to increase the strain hardening.[38,39]

In summary, we describe a methodology to synthesize bulk dense NS Ni samples with both high ductility and high strength. The cryomilling and QI forging employed in this study can be employed to synthesize many commercial NS metals and alloys as well as composites, and may be easily adapted to current industrial process and, hence, has the potential for large-scale application of NS materials. Our study also demonstrates that the significantly reduced processing artifacts and presences of a large fraction of equilibrium HAGBs and multi-/bimodal grain distributions are beneficial to the high ductility of NS materials. If the processing parameters are optimized, the ductility and strength can perhaps be improved even beyond the levels reported in this study.

Experimental

Cryomilling and QI Forge: Commercially pure Ni powder (−325 mesh) with a purity of >99.7 wt % was cryomilled using a Union Process Szegvari attritor in liquid nitrogen (ca. 77 K) at a rotation speed of 180 rpm for 16 h. Stainless steel balls with a diameter of 6.4 mm were used as the grinding medium, with a ball-to-powder mass ratio of 30:1. 0.2 wt % stearic acid ($CH_3(CH_2)_{16}COOH$) was used as a process-control agent. To obtain a bi-Ni sample, the as-received Ni powder was mixed with the 16 h cryomilled powders at the end of the milling. In an inert atmosphere glove box, the 150 g cryomilled Ni powders and the mixed powders were loaded into stainless steel cans with a length of 100 mm and an outer diameter of 40 mm. The powder contained in the stainless steel can was degassed under vacuum of about 10^{-3} Pa by a Varian Turbo-V 70D turbomolecular pump in a tube furnace at a first temperature of 450 °C for 24 h (ramped to 450 °C at 1 °C min^{-1}) and a second temperature of 810 °C for 2.5 h (ramped quickly from 450 to 810 °C). After degassing the cans were welded and cooled in air. The degassed cans were then heated to 800 °C at a heating rate of 1.5 °C min^{-1} for QI forging at AM^{2}T. The forged samples with a thickness of 20 mm and a diameter of 50 mm were finally cooled to room temperature in the air.

Mechanical Test: Dog-bone-shaped cylinder tensile specimens with a gauge length of 15 mm and a diameter of 3 mm were machined from the forged disks with a gauge direction perpendicular to the forging direction. Four tensile specimens were produced for each sample to obtain repeated results. The tensile tests were performed on an Instron 8801 universal testing machine (UTM) using Bluehill 2 software at a strain rate of $10^{-3}\,s^{-1}$ for the bi-Ni and CG Ni samples, and 10^{-2}, 10^{-3}, and $10^{-4}\,s^{-1}$ for the multi-Ni sample. The strain was measured by using a standard non-contacting video extensometer with a 100 mm field-of-view lens.

Microstructural Characterization: TEM observation was carried out on a Philips CM12 microscope operated at 100 kV, and high-resolution TEM was performed on a JEOL 2500 microscope operating at 300 kV. To prepare TEM specimens, small pieces were sectioned from the forged samples and polished into thin foils with thicknesses of about 50 μm. The thin foils were twin-jet electro-polished by a solution (75 vol % nitric acid + 25 vol % Methanol) for several minutes at a voltage of 7 V and a temperature of 235 K. The fracture surface was imaged by a FEI-XL30 SFEG scanning electron microscope using a 25 kV beam. The EBSD samples were vibratory polished using diamond suspension with a final particle size of 0.25 μm and then microetched by an etchant of 50 vol % nitric acid and 50 vol % glacial acetic acid. The EBSD scans were performed using a TSL OIM system on a Philips XL30 FEG SEM with step sizes of 75 nm or 130 nm. The densities of the multi- and bi-Ni samples were measured using an AG204 Mettler Toledo Balance at room temperature. Ethanol was used as auxiliary liquid to avoid bubbles on the sample surface. A thermometer was used to measure the temperature of the ethanol, from which its density was determined. The density of a pure Ni reference (with a purity of 99.99%) was measured as 8.91 g cm^{-3}.

Received: January 23, 2008
Revised: February 9, 2008
Published online: June 19, 2008

[1] C. C. Koch, D. G. Morris, K. Lu, A. Inoue, *MRS Bull.* **1999**, *24*, 54.
[2] H. Gleiter, *Prog. Mater. Sci.* **1989**, *33*, 223.
[3] J. R. Weertman, in *Nanostructured Materials: Proceeding, Properties and Applications* (Ed.: C. C. Koch), William Andrews, Norwich, NY **2002**, *p. 397.*
[4] a) C. C. Koch, *Scr. Mater.* **2003**, *49*, 657. b) E. Ma, *Scr. Mater.* **2003**, *49*, 663.

 © 2008 WILEY-VCH Verlag GmbH & Co. KGaA, Weinheim

[5] C. C. Koch, K. M. Youssef, R. O. Scattergood, K. L. Murty, *Adv. Eng. Mater.* **2005**, *7*, 787.
[6] E. Ma, *JOM* **2006**, *58(4)*, 49.
[7] Y. Wang, M. Chen, F. Zhou, E. Ma, *Nature* **2002**, *419*, 912.
[8] K. X. Tao, H. Choo, H. Q. Li, B. Clausen, J. E. Jin, Y. K. Lee, *Appl. Phys. Lett.* **2007**, *90*, 101911.
[9] F. D. Torre, H. V. Swygenhoven, M. Victoria, *Acta Mater.* **2002**, *50*, 3957.
[10] R. Schwaiger, B. Moser, M. Dao, N. Chollacoop, S. Suresh, *Acta Mater.* **2003**, *51*, 5159.
[11] Y. M. Wang, S. Cheng, Q. M. Wei, E. Ma, T. G. Nieh, A. Hamza, *Scr. Mater.* **2004**, *51*, 1023.
[12] F. D. Torre, P. Spatig, R. Schaublin, M. Victoria, *Acta Mater.* **2005**, *53*, 2337.
[13] F. D. Torre, H. V. Swygenhoven, R. Schaublin, P. Spatig, M. Victoria, *Acta Mater.* **2005**, *53*, 23.
[14] W. M. Yin, S. H. Whang, R. A. Mirshams, *Acta Mater.* **2005**, *53*, 383.
[15] C. Gu, J. Lian, Z. Jiang, Q. Jiang, *Scr. Mater.* **2006**, *54*, 579.
[16] C. Gu, J. Lian, Q. Jiang, *Scr. Mater.* **2007**, *57*, 233.
[17] T. R. Lee, C. P. Chang, P. W. Kao, *Mater. Sci. Eng.* **2005**, *A408*, 131.
[18] N. Krasilnokov, W. Lojkowski, Z. Pakiela, R. Valiev, *Mater. Sci. Eng.* **2005**, *A397*, 330.
[19] Z. I. Dzneladze, R. P. Shchegoleva, V. M. Afonia, V. F. Lykova, L. S. Golubeva, *Poroshk. Metall. (Kiev)* **1975**, *7*, 83.
[20] V. L. Tellkamp, A. Melmed, E. J. Lavernia, *Metall. Mater. Trans. A* **2001**, *32*, 2335.
[21] R. Z. Valiev, R. K. Isamgaliev, I. V. Alexandrov, *Prog. Mater. Sci.* **2000**, *45*, 103.
[22] K. M. Youssef, R. O. Scattergood, K. L. Murty, J. A. Horton, C. C. Koch, *Appl. Phys. Lett.* **2005**, *87*, 091904.
[23] L. Lu, Y. Shen, X. Chen, L. Qian, K. Lu, *Science* **2004**, *304*, 422.
[24] Y. H. Zhao, J. F. Bingert, X. Z. Liao, B. Z. Cui, K. Han, A. Sergueeva, A. K. Muhkerjee, R. Z. Valiev, T. G. Langdon, Y. T. Zhu, *Adv. Mater.* **2006**, *18*, 2949.
[25] Z. Horita, K. Ohashi, T. Fujita, K. Kaneko, T. G. Langdon, *Adv. Mater.* **2005**, *17*, 1599.
[26] Y. H. Zhao, X. Z. Liao, S. Cheng, E. Ma, Y. T. Zhu, *Adv. Mater.* **2006**, *18*, 2280.
[27] G. He, J. Eckert, W. Loeser, L. Schultz, *Nat. Mater.* **2003**, *2*, 3.
[28] B. B. Sun, M. L. Sui, Y. M. Wang, G. He, J. Eckert, E. Ma, *Acta Mater.* **2006**, *54*, 1349.
[29] Y. H. Zhao, Y. T. Zhu, X. Z. Liao, Z. Horita, T. G. Langdon, *Appl. Phys. Lett.* **2006**, *89*, 121906.
[30] Y. M. Wang, E. Ma, *Appl. Phys. Lett.* **2003**, *83*, 3165.
[31] Y. M. Wang, E. Ma, R. Z. Valiev, Y. T. Zhu, *Adv. Mater.* **2004**, *16*, 328.
[32] W. P. Lichti, A. F. Hofstatter, *US Patent* 4539175 **1985**.
[33] J. J. Thornton, B. Q. Han, E. J. Lavernia, *Metall. Mater. Trans. A* **2007**, *38*, 1343.
[34] Z. F. Zhang, J. Eckert, *Phys. Rev. Lett.* **2005**, *94*, 094301.
[35] J. Y. Huang, Y. T. Zhu, H. G. Jiang, T. C. Lowe, *Acta Mater.* **2001**, *49*, 1497.
[36] R. Z. Valiev, E. V. Kozlov, Y. F. Ivanov, J. Lian, A. A. Nazarov, B. Baudelet, *Acta Metall. Mater.* **1994**, *42*, 2467.
[37] Y. H. Zhao, J. F. Bingert, Y. T. Zhu, X. Z. Liao, R. Z. Valiev, Z. Horita, T. G. Langdon, Y. Z. Zhou, E. J. Lavernia, *Appl. Phys. Lett.* **2008**, *92*, 081903.
[38] M. Y. Gutkin, I. A. Ovid'ko, N. V. Skiba, *J. Phys. D* **2005**, *38*, 3921.
[39] N. Q. Chinh, P. Szommer, Z. Horita, T. G. Langdon, *Adv. Mater.* **2006**, *18*, 34.

© 2008 WILEY-VCH Verlag GmbH & Co. KGaA, Weinheim